

# UC Berkeley

## Controls and Information Technology

### Title

Performance analysis of pulsed flow control method for radiant slab system

### Permalink

<https://escholarship.org/uc/item/31s4x6jr>

### Authors

Tang, Haida  
Raftery, Paul  
Liu, Xiaohua  
[et al.](#)

### Publication Date

2018

### DOI

10.1016/j.buildenv.2017.11.004

### Supplemental Material

<https://escholarship.org/uc/item/31s4x6jr#supplemental>

### Data Availability

The data associated with this publication are in the supplemental files.

### Copyright Information

This work is made available under the terms of a Creative Commons Attribution-NonCommercial-ShareAlike License, available at <https://creativecommons.org/licenses/by-nc-sa/4.0/>

Peer reviewed

---

# Performance analysis of pulsed flow control method for radiant slab system

Haida Tang<sup>a</sup>, Paul Raftery<sup>b</sup>, Xiaohua Liu<sup>a,\*</sup>, Stefano Schiavon<sup>b</sup>, Jonathan Woolley<sup>b</sup>,  
Fred S. Bauman<sup>b</sup>

<sup>a</sup> *Department of Building Science, Tsinghua University, Beijing 100084, China*

<sup>b</sup> *Center for the Built Environment, University of California, Berkeley, CA, USA*

**Abstract:** We present a novel pulsed flow control method (PFM) using a two-position valve to regulate the capacity of radiant slab systems. Under PFM, the on-time duration of the valve is short (compared to all prior work, e.g. 4-minute), and fixed, while the off-time varies. We present a novel, open-source, finite difference model that assesses three-dimensional transient slab heat transfer, accounting for the transient heat storage of the pipe fluid. Sensitivity analysis results indicate the dominant factors influencing energy performance of the PFM are: on-time duration; pipe diameter; and spacing. We experimentally validated both the new control strategy and model in full-scale laboratory experiments. Compared with previous intermittent control strategies (with on-time durations over 30 min), at 50% part load the PFM reduces 27% required water flow rate and increases supply to return water temperature differential. Compared with the variable temperature control method, at 50% part load the PFM reduces 24% required water flow rate. The energy performance of PFM is comparable to that of a conventional variable flow rate control. However, it has more accurate capacity control, achieves a more uniform surface temperature distribution, and reduces initial investment by substituting two-position for modulating valves, thus showing promise for engineering applications.

**Keywords:** Radiant slab system; Pulsed flow control method; Laboratory experiment; 3D numerical model; Energy performance; Sensitivity analysis

---

\* Corresponding author: *Xiaohua Liu*

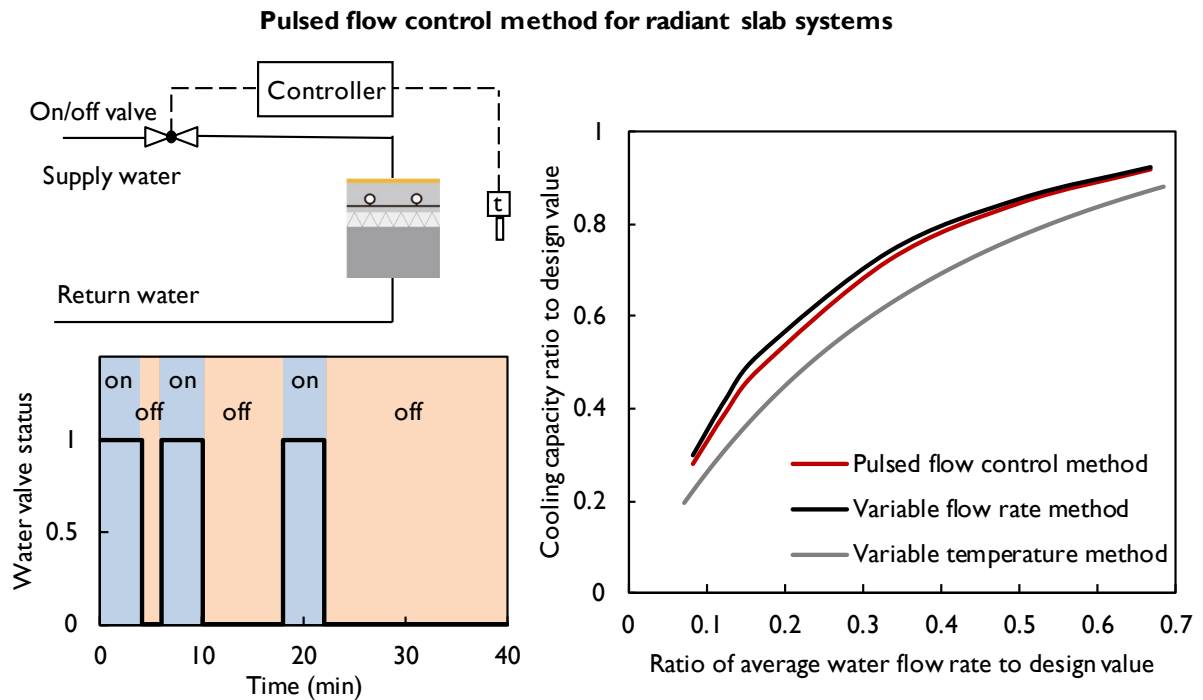
Department of Building Science, Tsinghua University, Beijing 100084, China

Tel: 8610-6277-3772

Fax: 8610-6277-0544

E-mail address: [lxh@mail.tsinghua.edu.cn](mailto:lxh@mail.tsinghua.edu.cn)

## Graphical abstract



## Nomenclature

$a$	Thermal diffusivity ( $\text{m}^2/\text{s}$ )
$c_p$	Specific heat ( $\text{J}/(\text{kg}\cdot\text{K})$ )
$d_i$	Inner diameter of pipe (m)
$d_o$	Outer diameter of pipe (m)
$EE$	Elementary effect of a design parameter (-)
$F$	Water flow rate ( $\text{m}^3/\text{s}$ )
$H$	Thickness of radiant floor (m)
$h_w$	Convective heat transfer coefficient in pipes ( $\text{W}/(\text{m}^2\cdot\text{K})$ )
$h_f$	Heat transfer coefficient of convection and longwave radiation ( $\text{W}/(\text{m}^2\cdot\text{K})$ )
$L_1$	Pipe spacing (m)

---

$P$	Period in PFM (s)
$q_s$	Floor surface heat flux ( $\text{W}/\text{m}^2$ )
$R_d$	Thermal resistance of the pipe wall ( $(\text{m}^2 \cdot \text{K})/\text{W}$ )
$T$	Temperature ( $^{\circ}\text{C}$ )
$T_{w,i}$	Chilled water temperature in the $i$ th water pipe ( $^{\circ}\text{C}$ )
$T_{w,s}$	Supply water temperature ( $^{\circ}\text{C}$ )
$T_z$	Indoor operative temperature ( $^{\circ}\text{C}$ )
$\Delta_i$	A predefined step in Morris method (-)
$\Delta T_w$	Supply and return water temperature difference ( $^{\circ}\text{C}$ )
$\Delta T_{s,diff}$	Surface temperature non-uniformity ( $^{\circ}\text{C}$ )
$v_w$	Water velocity in pipes (m/s)

#### Greek symbols

$\varphi$	Ratio of floor surface heat capacity (-)
$\xi$	Ratio of water flow rate (-)
$\lambda$	Thermal conductivity ( $\text{W}/(\text{m} \cdot \text{K})$ )
$\tau$	Time (s)
$\rho$	Density ( $\text{kg}/\text{m}^3$ )
$\mu$	Average of the elementary effect (-)
$\sigma$	Standard deviation of the elementary effect (-)

#### Subscripts

<i>on</i>	On-time duration
<i>off</i>	Off-time duration

---

<i>cyc</i>	One control cycle
<i>ref</i>	Reference case
<i>w</i>	Water

## 1 Introduction

Radiant slab heating and cooling systems including embedded surface systems (ESS) and thermally activated building systems (TABS), rely on pipes to distribute heated/cooled water throughout a building. These systems have gained appreciable interest and success for a variety of applications in new buildings and renovations [1,2]. Radiant slab systems are widely used due to their utility, energy efficiency, and aesthetics [3]. With the help of the low temperature difference between the floor surface and indoor air, a radiant slab achieves high temperature cooling and low temperature heating in buildings. This greatly increases the feasibility of using a broad range of more efficient cooling sources, such as cooling towers and ground water [4,5]. Compared with a conventional all-air system, radiant cooling systems can achieve energy savings by increasing the efficiency of cooled water generation and reducing transport energy consumption [6–11]. Besides, radiant systems provide equal or better comfort than all-air systems [12,13].

Field test results show that 20%-30% of thermal energy is wasted because of poor heating system regulation in China [14]. Therefore, numerous control methods have been suggested or applied to radiant slab systems. Under optimum operating conditions, the room with the highest load density, operating at maximum flow, should determine the supply water temperature leaving the cooling/heating plant for the building. Yet, many other rooms in the building have lower loads and do not require the extreme supply temperatures. Thus, each individual zone in the building requires a control method to handle these part load conditions. These methods can be broadly classified into supply water temperature control and water flow rate control.

### ***Supply water temperature control with constant flow rate***

In this case, a three-way mixing valve controls the supply temperature into each zone by injecting water into a recirculation loop with a constant speed pump. As shown in Fig. 1(a), the variable temperature control method (VTM) allows each room to have independent control over supply water temperature, and to maintain effective control of room conditions. It has a high control precision on the capacity over a wide range of part loads and also yields a relatively uniform surface temperature distribution across the slab. However, the exergy destruction of a mixing process between the supply and return water fluids degrades the energy efficiency of the heating/cooling plant. The VTM also comes with a high transport (pumping) energy cost due to the constant speed pump.

### ***Flow rate control with constant supply water temperature***

Two types of control methods are used to manipulate water flow rate. The first

---

one is a variable flow rate control method (VFM) equipped with a proportional (i.e. modulating) valve (see Fig. 1(b)). It maintains design conditions via a proportional integral control or an augmented constant gain control [15]. However, according to the experiment conducted by Jin et al. [16], the cooling capacity of the radiant slab ranges from 35.5 to 39.5 W/m<sup>2</sup> with a varying water flow rate from 0.096 to 0.581 m<sup>3</sup>/h. The effect of the water flow rate on the capacity of the radiant slabs is not great within this range of flows, even though the flow is laminar; only lower flow rates show significant differences in capacity. However, the proportional valve has a low control precision at low flows, and thus also on capacity, which in turn results in overcooling/overheating at part loads [17]. Furthermore, due to the relatively high initial cost of the modulating valve and the precision actuator in both of the VTM and VFM, developers and heating companies often simplify indoor systems by using manual regulating valves [18]. It has a negative influence on energy efficiency and is detrimental to regulating heat use.

The second method, i.e., intermittent control, which supplies water by intermittently fully opening or fully closing a two-position valve (see Fig. 1(c)), is widely spread attributed to the low initial costs. Previous studies proposed and investigated many intermittent control methods, including conventional on-off control, fuzzy logic-based on-off control [19], two-parameter switching control [20], pulse width modulation [21,22], and model predictive intermittent control [23,24]. However, these intermittent control strategies cited here all have relatively long valve open phases, ranging from 30 min to several hours that are comparable to the response time (at 63.2% of the steady state value) of the radiant slab. As a result, they are found to yield large changes in the floor surface temperature as well as indoor operative temperature [25].

Inspired by the possibility of using the high thermal inertia of radiant slabs to mitigate the effects of relatively high frequency water temperature fluctuation, we propose a novel pulsed flow control method (PFM) based on intermittent control with a fixed and short on-time duration (4 minutes or less). This is far less than the response time of the slab, implying that the periodic steady state results will not vary significantly due to the pulsed nature of the flow. We then use varying off-time duration to allow for control of flow to very low part loads. The key difference from all intermittent control strategies published before is that the proposed approach is designed with an on-time duration less than or equal to the time taken to replace the stored water in pipes.

To address the dynamic behavior of a radiant slab in the pulsed flow control, the transient heat transfer processes need to be considered in numerical simulation. The finite difference method and finite element method are typically used to calculate the radiant slabs with a two-dimensional heat conduction problem [26,27]. The RC-network model and heat conduction transfer function method are two representative simplified heat transfer models [28–31] and they are used in TRNSYS 18.0 and EnergyPlus 8.2.0, respectively. The 2D heat conduction model and the RC-network model of the radiant slab simplify the water temperature into one node, i.e., the average of the supply and return water temperature, and ignore the heat

storage of the water in the pipe. However, in the short on-time duration of the PFM, the cooled water flushes the pipe, yielding a changing non-linear water temperature distribution along the pipe from the inlet to outlet; in the off-time duration, the water in the pipe continues exchanging heat with the radiant slab. As a result, previous models cannot capture the transient change of the water temperature distribution along the pipe in the PFM. A more detailed model for the radiant slab capable of investigating the transient, 3-dimensional effects, and the heat storage effect of the pipe fluid, is still absent.

The main objective of this paper is to evaluate the performance and regulation characteristics of this pulsed flow control method and judge how it compares to the existing approaches in terms of control precision, required water flow rate, supply and return water temperature difference, and surface temperature uniformity in part loads. We developed a three-dimensional numerical model for radiant slabs in order to capture the water temperature difference along the pipe from inlet to outlet, discretized by the finite difference method, and used it to simulate the dynamic behavior of the PFM. Furthermore, we experimentally tested and validated both the new control strategy and the new numerical model in full-scale laboratory experiments. This study is beneficial for the design and optimization of the PFM in engineering applications.

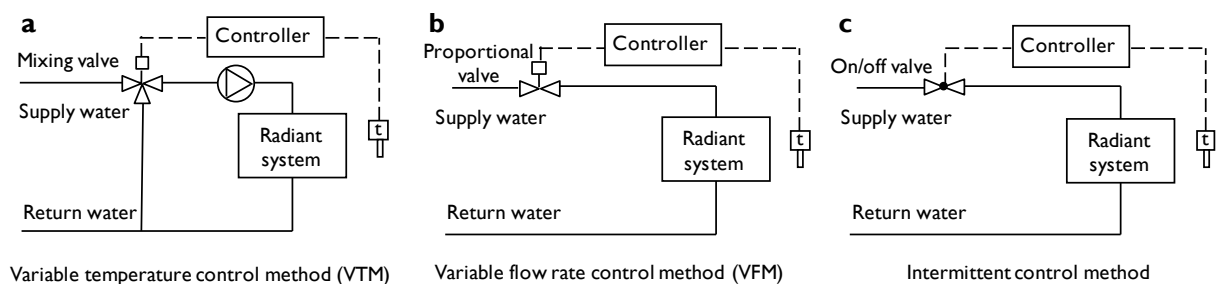


Fig. 1 Schematic of control methods for a radiant system: (a) Variable temperature control method (VTM); (b) Variable flow rate control method (VFM); and (c) intermittent control method.

## 2 Pulsed flow control method

### 2.1 Description of control method

A pulsed flow control method uses a low cost two-position valve and actuator to regulate the capacity of a radiant slab floor. Compared to the variable flow method, it does not require a modulating valve or precision actuator. In order to achieve a large supply and return water temperature difference with a small water flow rate, the on-time duration ( $P_{on}$ ) is designed fixed while the off-time duration ( $P_{off}$ ) is variable and ranges from 0 to over 10 times of the on-time duration. The control period ( $P_{cyc}$ ) of PFM is the sum of the on-time and off-time durations. Describing how this functions in a cooling mode, during the off-time duration, the water in the pipe

continues to absorb heat. Then, during the fixed and short on-time duration, the supplied cooled water flushes the water pipe and replaces the stored water in the pipe in order to obtain a high return water temperature. A high return water temperature is beneficial for improving the efficiency of the cooling plant.

The geometric and thermal parameters of different radiant slabs vary from case to case, resulting in a wide range of thermal resistances and response times. Therefore, we introduce a non-dimensional analysis to compare the performance of different radiant slab floors. A continuous flow control (CFM) with a fixed water flow rate is denoted as the reference case. The non-dimensional index is defined as the ratio between the time-weighted average result of PFM in a periodic steady state and that of the reference case. Therefore, the cooling/heating capacity ratio ( $\varphi$ ) and ratio of design water flow rate ( $\xi$ ) are expressed as Eq. (1) and (2), respectively. For the VTM, the ratio of design water flow rate in part load is the ratio between the water flow rate in the primary loop and the design value. The supply and return water temperature difference ( $\Delta T_w$ ) is calculated according to Eq. (3).

$$\varphi = \frac{1}{q_{s,ref} P_{cir}} \int_0^{P_{cir}} q_s(\tau) d\tau \quad (1)$$

$$\xi = \frac{1}{F_{ref} P_{cir}} \int_0^{P_{on}} F_{on}(\tau) d\tau \quad (2)$$

$$\Delta T_w = \frac{1}{P_{on}} \int_0^{P_{on}} (T_{w,r} - T_{w,s}) d\tau \quad (3)$$

where  $q_s$  is the real-time floor surface heat flux in a periodic steady state of PFM;  $F_{on}$  is the water flow rate in the on-time duration;  $q_{s,ref}$  and  $F_{ref}$  are floor surface heat flux and water flow rate of the reference case, respectively.

In the cooling condition, surface temperature non-uniformity plays a significant role in the condensation risk of radiant systems [32]. Condensation is most likely to occur at the point with the lowest surface temperature. We quantify the floor surface temperature non-uniformity ( $\Delta T_{s,diff}$ ) using the time-weighted average difference between the maximum and minimum surface temperature.

$$\Delta T_{s,diff} = \frac{1}{P_{cyc}} \int_0^{P_{cyc}} (\max(T_s) - \min(T_s)) d\tau \quad (4)$$

## 2.2 Experimental facilities and procedure

We performed an experiment during October 2016 in a full-scale test chamber in the Department of Energy's FLEXLAB at Lawrence Berkeley National Laboratory (Fig. 2) in order to evaluate the performance of the pulsed flow control method [33]. The dimensions of the environmental chamber are 6.1 m by 9.3 m by 3 m high (170 m<sup>3</sup>). The chamber has a radiant slab floor and an overhead air supply system. Fig. 2(a) and (b) show the layout of the chamber as we set it up for the experiment. We blocked

the windows with opaque thermal insulation for this validation experiment. The thermal insulation has a thickness of 100 mm and a thermal conductivity of 0.04 W/(m·K). The external walls of the environmental chamber are well insulated, with a built-in 200 mm thick layer of thermal insulation (thermal conductivity  $\lambda=0.04$  W/(m·K)). Thus, we eliminated the majority of external heat transfer disturbances, including solar radiation and conduction to the outdoor air.

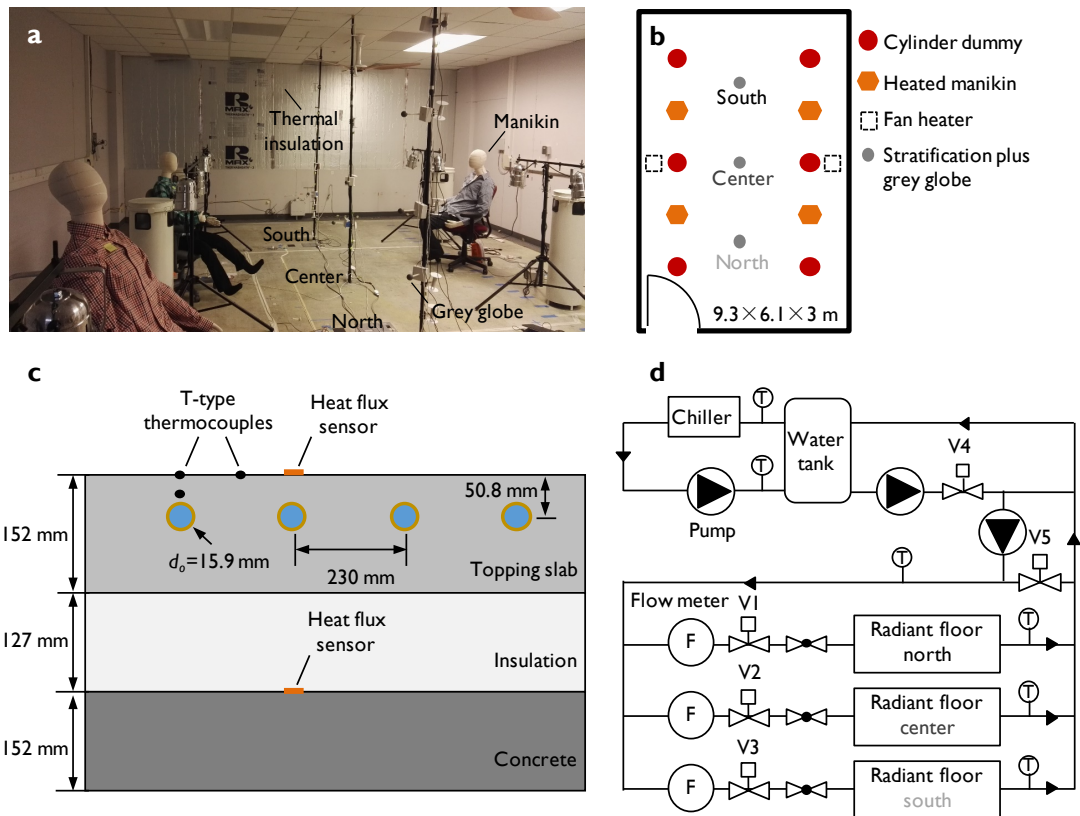


Fig. 2 Experimental facilities and instruments: (a) Internal view of the full-scale experimental chamber; (b) layout of the chamber; (c) structure of the radiant slab system; and (d) schematic of chilled water system.

Fig. 2(c) shows the cross-section of the radiant slab floor. Polyethylene pipes were embedded in a 152 mm thick light concrete core with a thickness from the pipe center to the floor surface of 50.8 mm. The bottom surface of the topping slab was attached to a 127 mm thick extruded polystyrene layer. The topping slab: thermal conductivity 0.75 W/(m·K), density 1282 kg/m<sup>3</sup>, specific heat 837 kJ/(kg·K). The thermal insulation: thermal conductivity 0.035 W/(m·K), density 265 kg/m<sup>3</sup>, specific heat 1300 kJ/(kg·K). The bottom concrete: thermal conductivity 1.311 W/(m·K), density 2240 kg/m<sup>3</sup>, specific heat 836.8 kJ/(kg·K). The average pipe spacing was 230 mm with very few pipe spacing deviating a bit. The pipe diameter was 14.3 mm/15.9 mm. T-type thermocouples (TJ36, OMEGA, US) and heat flux sensors (PHFS-09e, FluxTeq, VA, US) were located on the floor surface above the pipe and in the middle of two adjacent pipes in order to measure the average radiant floor surface temperature and heat flux, respectively. In addition, a heat flux sensor (PHFS-09e,

---

FluxTeq, VA, US) was located on the bottom surface of the thermal insulation. We logged temperature and heat flux continuously at one-minute sampling intervals. Fig. 2(d) shows the schematic of the chilled water system of the experimental platform. The primary water loop included a buffer water tank and the temperature in the tank was roughly controlled by the chiller around 8 °C. In the secondary water system, a mix of the chilled water from the water tank and the return water was supplied to radiant slab floors. A proportional valve (V4) regulated the mixing ratio through a PID control loop in order to maintain the supply water temperature at 12 °C more precisely than would be possible with the primary loop alone. The low supply water temperature was utilized to enlarge the difference of cooling capacities between various experimental conditions, preventing the instrumental error from concealing the variation between experimental conditions.

The radiant slab floor had three separate parts (south, center and north) which are controlled by three proportional valves (V1, V2 and V3), respectively. These three proportional valves were open and closed simultaneously in the condition of the pulsed flow control. During the on-time duration, V1, V2 and V3 were open to their pre-defined opening values with V5 closed. During the off-time duration, V1, V2 and V3 were closed with V5 open for bypass. We measured the supply and return water temperatures of each radiant terminal using immersion RTDs (P-M-A-1, OMEGA, USA) with -29 to 100 °C measuring range,  $\pm 0.1$  °C uncertainty, and measured the water flow rate of each radiant terminal using a water flow meter (Sitrans F M MAG 1100, Siemens, Germany) with 0 to 10 m/s measuring range, 0.2% uncertainty.

We placed six cylinder dummies (designed according to DIN 14240), four heated manikins and two fan heaters with a total electric power of 3300 W in the environmental chamber, representing a total cooling load density of 58 W/m<sup>2</sup> (see Fig. 2(b)). The internal heat gains comprise an occupant density of 0.25 person/m<sup>2</sup>, a lighting power density of 20 W/m<sup>2</sup>, an equipment power density of 20 W/m<sup>2</sup>, representing the cooling load of an office. We located three grey globe temperature sensors (F2020-1000-B-100, OMEGA, US) at heights of 0.6, 1.1 and 1.7 m in the chamber to monitor the indoor operative temperature. We maintained a constant operative temperature of 24 °C at a height of 1.1 m using the auxiliary overhead air system. The overhead air system has a constant air flow rate of 2600 m<sup>3</sup>/h and a variable supply air temperature to control the operative temperature in different experimental conditions.

We conducted experiments of the pulsed flow control method and continuous flow control method to compare their performance. Table 1 describes the experimental conditions. We evaluated three experimental conditions of the PFM with various on and off time durations. Each part of the radiant slab floor (south, center and north) in the experimental chamber had two or three water loops with a pipe length ranging from 35 to 52 m. The design water flow rate of each loop during the on-time duration in PFM was designed and balanced at 0.10 m<sup>3</sup>/h. Given this flow rate and the diameter of the pipe, it takes 3-5 min for the chilled water to flush the water from the pipe (the variation is due to differing pipe lengths from the control valve). In PFM I and II, we set an on-time duration of 4 min around the duration taken

to replace the stored water in pipes and different off-time duration to evaluate the cooling capacity in PFM. In PFM III, we set an on-time duration of 29 min that is much longer than the duration to flush the water. The effect of on-time duration on the cooling capacity is evaluated through the comparison between PFM II and III. In addition, we conducted an experimental condition of the constant flow control method (CFM) with a water flow rate of 0.10 m<sup>3</sup>/h as a reference case. Steady state for the CFM and the periodic steady state for the PFM were defined as a difference of less than 0.1 °C between the recent floor surface temperature against that 4 hours prior.

Table 1 Experimental conditions

Condition	On time min	Off time min	Design flow rate m <sup>3</sup> /h	Average flow rate m <sup>3</sup> /h (%)
PFM I	4	26	0.092	0.012 (11)
PFM II	4	6	0.093	0.037 (35)
PFM III	29	31	0.103	0.050 (47)
CFM	NA	NA	0.106	0.106 (100)

### 2.3 Experimental results

Fig. 3(a) and (b) shows the temperature variation during a periodic steady state in PFM I with 4 min on / 26 min off. As Fig. 3(a) shows, even with such a small ratio of the design water flow rate ( $\zeta=0.11$ ), the fluctuation of the average surface temperature of the radiant slab system, i.e., the maximum minus minimum temperature during a control cycle, is less than 0.1 °C in periodic steady state conditions. The results reveal that the PFM yields a relatively constant surface heat flux due to the heat capacity of the water in the pipes and the much larger heat capacity of the slab construction material.

The experimental results demonstrate the feasibility of the PFM. Fig. 3(b) shows the supply and return water temperature change of PFM I. Though the supply water temperature set point was 12 °C, it frequently overshoot this due to the highly intermittent influence of the return water. It took several minutes for the PID loop to adjust the proportional valve (V4) to control the supply water temperature at the beginning of the on-time duration. The average supply water temperature was 12.3 °C over multiple control cycles in periodic steady state. As the duration to flush the water pipes ranged from 3 min to 5 min, the stored water in pipes was replaced during the on-time duration, resulting in a high return water temperature over 20 °C.

As the design water flow rate of CFM was the same as the PFM cases when the valve is open, we used the CFM as the reference case for the non-dimensional analysis. Fig. 3(c) and (d) shows the performance of the pulsed flow control method plotted as a function of the ratio of design water flow rate. According to Fig. 3(c), the PFM regulated the cooling capacity in a large range of part load. The cooling capacity of PFM II was 4% larger than that of PFM III, while the average flow rate in the whole period of PFM II was 0.037 m<sup>3</sup>/h, 35% lower than that of PFM III. A shorter on-time duration in a PFM requires a lower water flow rate to attain the same cooling capacity. Fig. 3(d) shows the comparison of supply and return water temperature differences ( $\Delta T_w$ ) between different control methods. In addition, different parts of the

radiant slab floor (south, center and north) with a variety of pipe lengths behaved similarly. The experimental results reveal that the pulsed flow control method achieved a high supply and return water temperature difference with a low average water flow rate in part load. Besides, the simulation results in Fig. 3(c) and (d) show the performance of the PFMs with an on-time duration of 4 min, which we describe in Section 3.2.

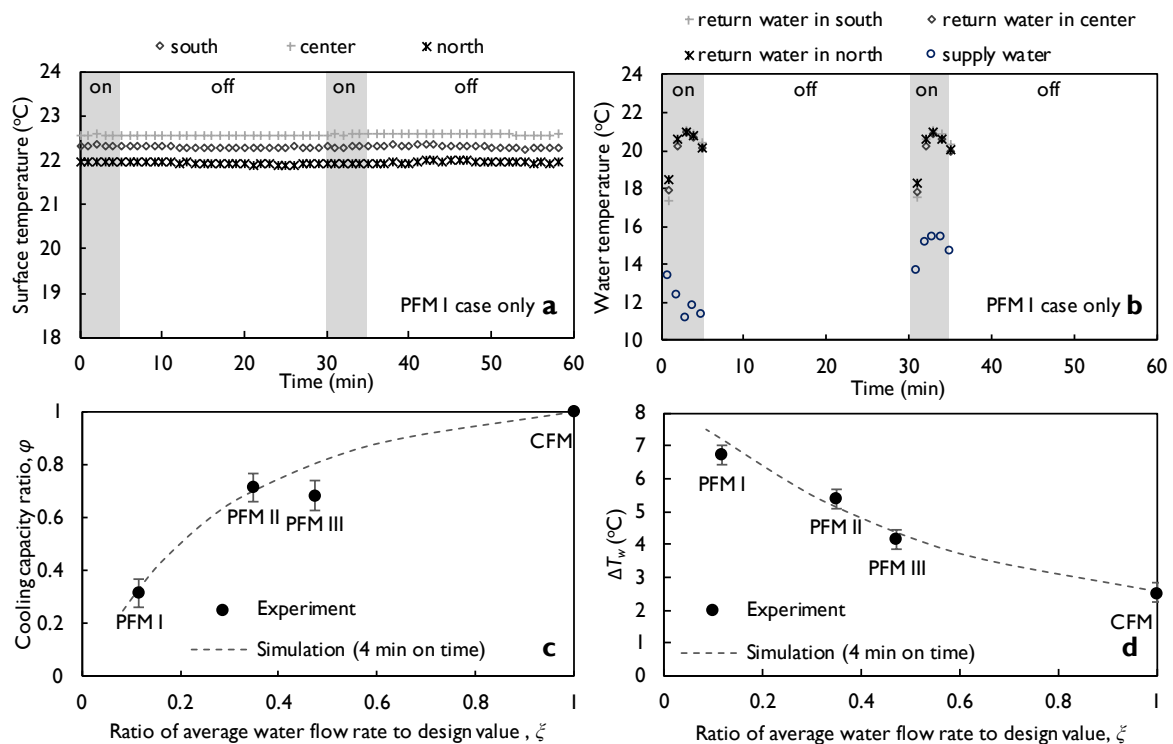


Fig. 3 Temperature variation during a periodic steady state in the pulsed flow control with 4 min on/ 26 min off (PFM I case): (a) Floor surface temperature; and (b) supply and return water temperature. (c) and (d) show the ratio of cooling capacity ( $\phi$ ) and supply and return water temperature difference ( $\Delta T_w$ ) of all three pulsed flow control cases (PFM I to III) as a function of the ratio of design water flow rate ( $\zeta$ ), with CFM as the reference case.

### 3 Simulation model

#### 3.1 Heat conduction model

We developed a three-dimensional numerical model of the radiant slab floor to capture the transient temperature distribution along the pipe from inlet to outlet, and the thermal storage effect of the static water in the pipe. Fig. 4 shows the structural representation of a typical radiant slab floor used in the 3D numerical model. Dynamic heat transfer in radiant floor systems includes heat exchange between cooled water, pipes, building structure and room thermal environment. To simplify the heat transfer process, the following assumptions are applied:

1) The heat exchange of the radiant slab surface consists of convection between the slab surface and indoor air and radiation between the slab surface and envelope internal surfaces. It is simplified into the heat transfer between the slab surface temperature and the operative temperature in the middle of the room.

2) The materials of each layer are homogeneous and their properties don't vary with temperature;

3) The pipe network layout is simplified into an array of parallel water pipes along  $z$  direction. In addition, the circular pipe is simplified into a rectangle pipe with the same perimeter[34].

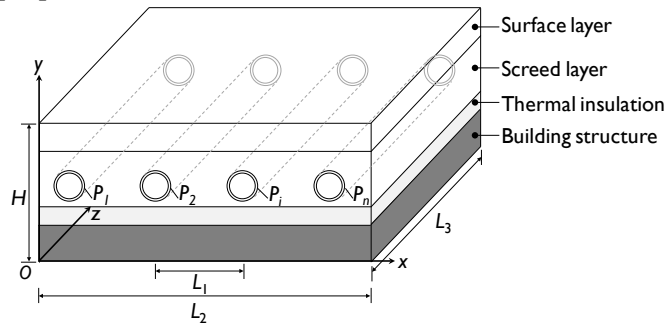


Fig. 4 Structural representation of a typical radiant slab.

A differential equation describing three-dimensional transient heat-conduction in an embedded-pipe slab floor is given in Eq. (4)

$$\frac{\partial T}{\partial \tau} = a \left( \frac{\partial^2 T}{\partial x^2} + \frac{\partial^2 T}{\partial y^2} + \frac{\partial^2 T}{\partial z^2} \right) \quad (5)$$

The boundary conditions of the governing equations are:

$$\left. \frac{\partial T}{\partial x} \right|_{x=0} = \left. \frac{\partial T}{\partial x} \right|_{x=L_2} = 0, \quad \left. \frac{\partial T}{\partial z} \right|_{z=0} = \left. \frac{\partial T}{\partial z} \right|_{z=L_3} = 0 \quad (6)$$

$$\lambda \left. \frac{\partial T}{\partial y} \right|_{y=H} = h_f (T_z - T), \quad \lambda \left. \frac{\partial T}{\partial y} \right|_{y=0} = -h_c (T_c - T) \quad (7)$$

$$\lambda \left. \frac{\partial T}{\partial n} \right|_{P_i} = (T_{w,i} - T) / (1/h_w + R_d) \quad \text{where } i = 1, 2, \dots, n \quad (8)$$

Where  $h_f$  and  $h_c$  are the heat exchange coefficient of convection and longwave radiation of the floor surface and the ceiling surface, respectively.  $T_z$  and  $T_c$  are the indoor operative temperature in the room and the room downstairs, respectively.  $R_d$  is the thermal resistance of the pipe wall, expressed as  $R_d = \ln(d_o/d_i)/(2\pi\lambda_d)$ .  $h_w$  is the convective heat transfer coefficient in pipes between the water and the pipe wall, calculated by the Dittus-Boelter equation [35].  $P_i$  is the outer pipe wall of the  $i$ th pipe and  $n$  is the number of water pipes in the radiant slab floor.

The governing equation of water in the pipes is

$$\frac{\partial T_{w,i}}{\partial \tau} + v_w \frac{\partial T_{w,i}}{\partial z} = \frac{4}{\rho_w c_{p,w} \pi d_i^2} \int_{P_i} (T - T_{w,i}) / (1/h_w + R_d) ds \quad (9)$$

where  $T_{w,i}$  represents the water temperature in the  $i$ th water pipe;  $v_w$  is the water velocity in the pipe.

The partial differential equation of 3D heat conduction in the radiant slab floor is discretized by finite difference using the Crank Nicolson method and solved by the fraction step method. The governing equation of chilled water is discretized by a first order upwind scheme. We carefully treated the different regions of the model in the meshing process to ensure that the meshes were sufficiently refined, and that the results were independent of the number of nodes. By comparing the simulated results under different mesh refinement levels, and considering the convergence and stability of the numerical calculation, we selected the refined mesh of approximately 200,000 cells to solve the heat conduction model. The source code of the 3D numerical model is included in the supplementary material.

There are limitations for this 3D model. This model assumes parallel lines of pipes and this is not always the way that the radiant slabs are laid out (e.g., counter flow spiral and reverse spiral return). This model also ignores the effect of an exterior wall and the adjacent radiant floor, and the thermal bridge that occurs at this location. The interaction effect between the building envelope and radiant floor is not taken account in this model. In addition, this model would not apply in the type of radiant floor with pipes embedded in wood planks or insulation panels and aluminum mounting flanges/fins used to increase heat transfer.

### 3.2 Model validation

We compared the experimental results of a radiant slab during the preheating period and the cool-down period measured by Wang et al. [27] with those of the 3D numerical heat conduction model in this paper. The structure of the radiant slab is the same as that in Fig. 4. Table 2 shows the geometric and thermal parameters of the radiant slab, as well as the response time defined in our previous study [36]. Fig. 4 shows the floor surface temperature simulated using the 2D model reported by Wang et al. [27], RC-network model reported by Ning et al. [36] and 3D model presented in this paper, along with the experimental values measured during the preheating period (see Fig. 5(a)) and during the cool-down period (see Fig. 5(b)). In the preheating period, the Mean Absolute Error and the Root Mean Squared Error between the 3D numerical simulation and the experimental values are 0.07 °C and 0.09 °C, respectively. Besides, in the cool-down period, the Mean Absolute Error and the Root Mean Squared Error of the 3D numerical model are 0.25 °C and 0.21 °C, respectively. In both of the preheating and cool-down period, the 3D numerical model fits better to the experimental results than the 2D model or the RC-network model. The good consistence in preheating and cool-down periods validates the accuracy of the 3D numerical model in valve on-time duration and valve off-time duration of the PFM.

Table 2 Structure and thermal properties of radiant slab.

Layer name	Material name	Wang et al. [27]				ASHRAE Handbook [37]			
		Density (kg/m <sup>3</sup> )	Conductivity (W/(m·K))	Specific heat (J/(kg·K))	Thickness (mm)	Density (kg/m <sup>3</sup> )	Conductivity (W/(m·K))	Specific heat (J/(kg·K))	Thickness (mm)
Surface layer	Tile (ceramic)	1900	1.1	1050	5	2300	1.3	840	9.5
Screed layer	Crushed stone and mortar	2300	1.51	920	50	1920	1.4	840	60
Pipes	Cross linked Polyethylene (PEX)	936	0.38	1470	$L_l = 300,$ $d_o = 20,$ $d_i = 16$	936	0.38	1470	$L_l = 155,$ $d_o = 19.1,$ $d_i = 14.6$
Thermal insulation	Glass fiber board	30	0.027	2000	50	160	0.032	1670	60
Building structure	Low-mass aggregate concrete.	1920	1.1	840	200	1920	1.1	840	200
Response time (h)	$\tau_{95} / \tau_{63.2}$	5.54 / 1.97				4.03 / 1.47			

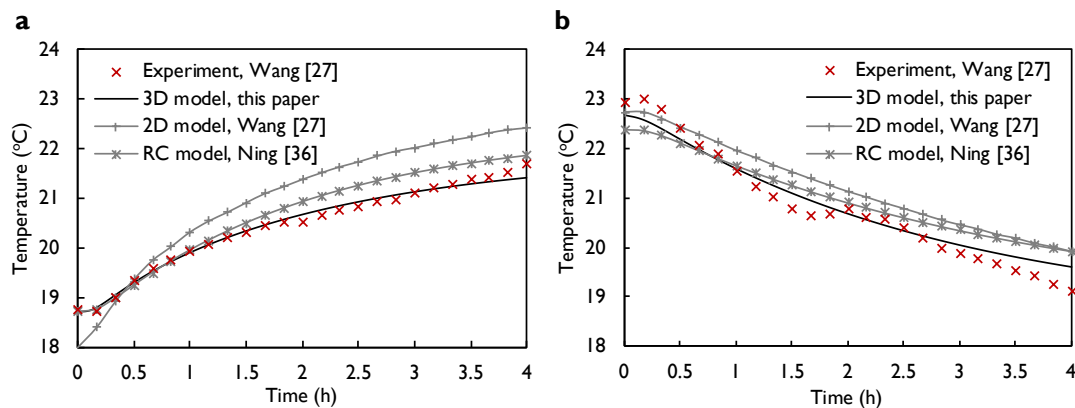


Fig. 5 Comparison between simulation and experimental values of the average floor surface temperature: (a) During the preheating period; and (b) during the cool-down period.

Furthermore, we simulated the performance of the radiant slab using the pulsed flow control method with an on-time duration of 4 min in the experiment described in section 2.2. The dashed line in Fig. 3(c) is the simulated cooling capacity ratio plotted as a function of the ratio of design water flow rate for the PFM. The dashed line in Fig. 3(d) is the simulated supply and return water temperature difference for the PFM. The simulation results agree well with the experimental values of the PFM I and PFM II that also have a 4 min on-time duration. Therefore, the 3D numerical model shows high accuracy for simulating the dynamic performance of the radiant slab under either the variable flow method or the pulsed flow control method.

---

## 4 Simulation results

### 4.1 Performance of a typical pulsed flow control

We chose a typical structure of a radiant slab from the ASHRAE handbook [37] (shown in Table 2) to study the transient effects of the pulsed flow control method. The pipe network layout has a length of 120 m and the thickness of the layer from pipe center to the lower layer of the screed is 15 mm. We simplified the thermal insulation and building structure into a steady state thermal resistance in simulation. The supply chilled water temperature and indoor operative temperature were 16 °C and 24 °C, respectively. As for the reference case of the continuous flow control method, the design water flow rate was 0.242 m<sup>3</sup>/h, resulting in a pressure drop of 18 kPa, a floor surface heat flux of 29.8 W/m<sup>2</sup>, and a supply and return water temperature difference of 2.1 °C. Under these conditions, it takes 5 minutes for the water to flush the pipe and entirely replace the water in the pipe. We simulated the dynamic behavior of a PFM designed with 4 min on / 8 min off using the 3D numerical model described above.

Fig. 6 compares the performances between the PFM, VFM and VTM with the same average water flow rate. Fig. 6(a) shows the floor surface and return water temperature change of the radiant slab during one control cycle in a periodic steady state. Despite the on-off nature of operation, the floor surface temperature is almost constant due to the thermal mass of the slab construction materials that have a response time ( $\tau_{95}$ ) of 4.03 h. The deviation of surface temperature between the PFM and the VFM was less than 0.08 °C. The return water temperature of the PFM decreased slightly with the on-time duration, which was different from the constant return water temperature in the VFM. This PFM attained a time-weighted average cooling capacity of 21.6 W/m<sup>2</sup>, while the VFM at the same average flow rate achieved 22.1 W/m<sup>2</sup>. This is 72% of the cooling capacity of the reference CFM, while requiring only 33% of the design water flow rate. The supply and return water temperature difference of the PFM was as high as 4.7 °C, comparable to that of the VFM (4.8 °C) and higher than that of the VTM (4.3 °C). Furthermore, Fig. 6(b) shows the detailed water temperature distribution along the pipe length at 2 min, 4 min, 8 min and 12 min intervals in a control cycle. Cooled water flushes the pipe and replaces the stored water during the on-time duration, resulting in a decrease of the pipe water temperature. At 2 min after the initial pulse, the cooled water has passed through half of the overall length of the pipe. The water in the pipe, which is static during the off phase, still extracts heat from the concrete core, increasing the temperature of the water, and then the cycle continues. The VTM has a smaller temperature difference along the pipe from inlet to outlet compared with the VFM and PFM. Fig. 6(c) shows the temperature distribution of the *x-y* section in the middle of radiant floor. Fig. 6(d) shows the surface temperature in *x-y* section average over one periodic steady state cycle in the PFM, VFM and VTM. The floor surface temperature non-uniformities of the PFM, VFM and VTM were 2.2 °C, 2.9 °C and 1.0 °C, respectively. Compared with the VFM, the PFM leads to a uniform surface temperature due to the pulsed

nature of the flow and the heat conduction in radiant slab during the off phase. The PFM achieves this while maintaining a similar overall cooling capacity with the same average flow rate. The VTM also achieves a uniform surface temperature resulting from its small water temperature difference along the pipe.

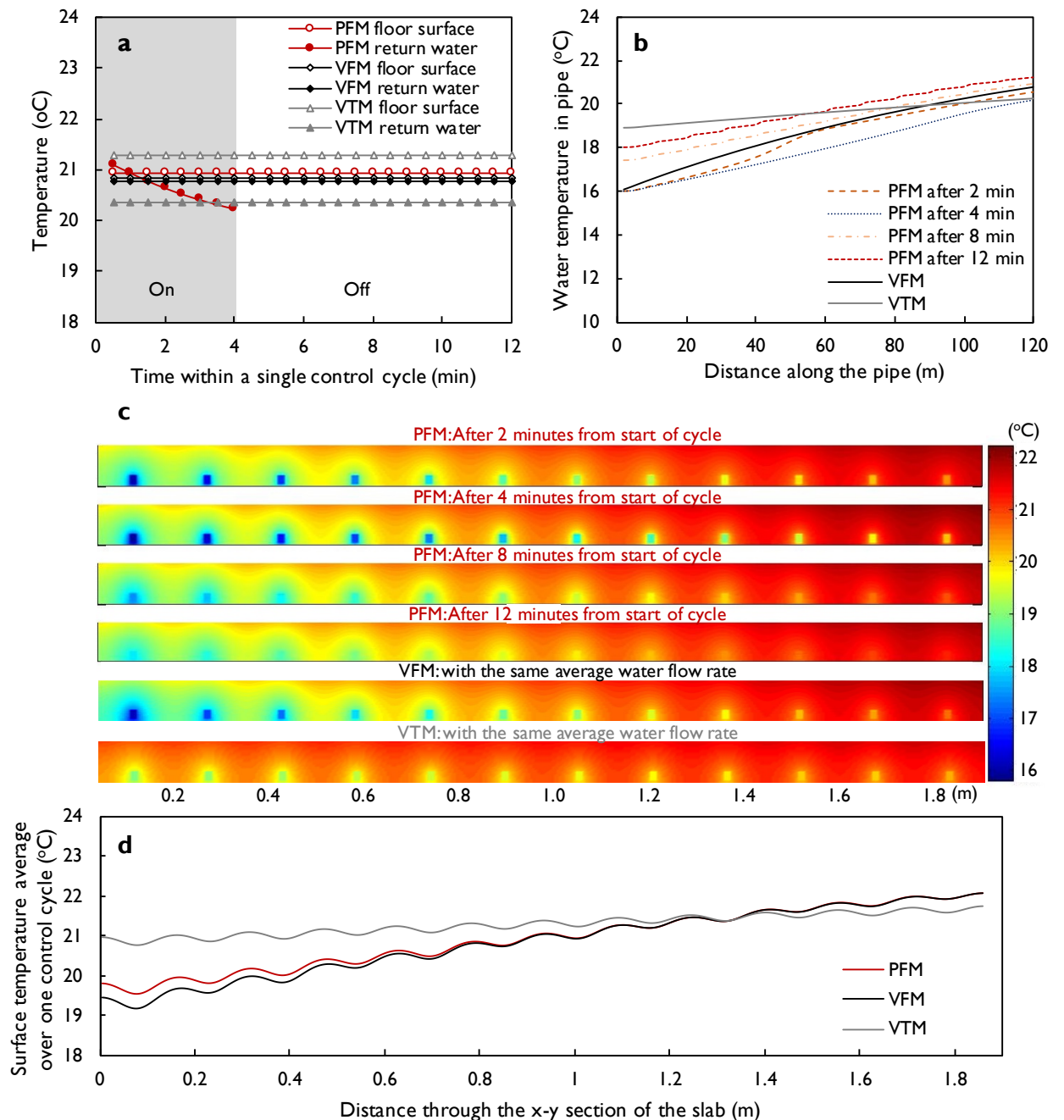


Fig. 6 Comparison of performance between a typical PFM with 4 min on/ 8 min off, a VFM and a VTM with the same average water flow rate and same supply water temperature (16 °C): (a) Floor surface and return water temperature change; (b) temperature distribution of pipe water; (c) temperature distribution of the radiant floor's x-y section at 2 min, 4 min, 8 min and 12 min intervals through one control cycle in PFM; and (d) surface temperature average over one control cycle.

---

## 4.2 Comparison of control methods

We compared the average cooling capacity, supply and return water temperature, and the surface temperature non-uniformity of the pulsed flow rate control method (PFM) in a periodic steady state with those of the variable flow rate control method (VFM) and variable temperature control method (VTM) in a steady state. The schematic of these three control methods of a radiant slab is shown in Fig. 1. Specifically, in the VTM, the supply water temperature to the radiant floor was controlled through a three-way mixing water valve to regulate the cooling capacity. The water flow rate of the primary loop (i.e. the water injected from the chilled water loop) in the VTM was variable and used to calculate the ratio of design water flow rate, while the secondary pump speed was fixed and the water flow rate through the radiant slab was assumed constant, at the design water flow rate. The PFM was designed with an on-time duration of 4 min and a variable off-time duration. The structure and design condition of the radiant slab used in comparison are the same with that in section 4.1.

Fig. 7(a) and (b) shows the comparison of energy performance between the three control methods. In Fig. 7(a), the capacity ratio of the PFM quite approaches to that of the VFM with the same average water flow rate. The PFM attained greater cooling capacity than the VTM with the same water flow rate. Fig. 7(b) shows the supply and return water temperature difference ( $\Delta T_w$ ) plotted as a function of the ratio of water flow rate.  $\Delta T_w$  of the VFM is highest, that of the PFM comes second, and that of the VTM is lowest. To achieve a cooling capacity ratio of 50%, the ratios of the required water flow rate for the VFM, PFM and VTM were 15.9%, 17.7% and 23.4%, respectively. Meanwhile, the supply and return water temperature differences of the VFM, PFM and VTM were 6.7 °C, 6.1 °C and 5.1 °C, respectively. It is difficult for a proportional valve to regulate the ratio of water flow rate below 15% precisely [17]. This 15% flow rate value corresponds to approximately 50% capacity, indicating that the VFM cannot regulate capacity precisely in this region. In contrast, the PFM could regulate the cooling capacity better in part load through accurate control of the off-time duration. Fig. 7(c) shows the comparison of surface temperature non-uniformity ( $\Delta T_{s,diff}$ ). As for the VFM, the low flow rate in part load results in a large temperature difference along the pipe length from the inlet to outlet, which exacerbates the non-uniformity of the surface temperature. As for the PFM, the long off phase in part load benefits the heat conduction of the surface layer, which maintains a uniform surface temperature in part load. The VTM achieves the lowest non-uniformity of the surface temperature. Furthermore, the non-uniformity in the VTM decreases with the decreasing water flow rate.

Compared with the VTM, the PFM requires 24% lower water flow rate and increases the supply and return water temperature difference by 1.0 °C at a capacity ratio of 50%. Thus, when compared to the VTM, the PFM will reduce pumping power of the overall system, while also providing higher return temperatures to allow for more efficient operation of cooling plant. Furthermore, the flow rate (and significant associated additional pumping power) of the radiant terminal in the VTM that was

constant in part load was not included. The actual energy performance of the VTM is worse than that plotted in Fig. 7(a). Therefore, the pulsed control method achieves a high supply and return water temperature difference, a low water flow rate and a relatively uniform floor surface temperature in part load. Nevertheless, the VTM achieves a high surface temperature uniformity in the same part load.

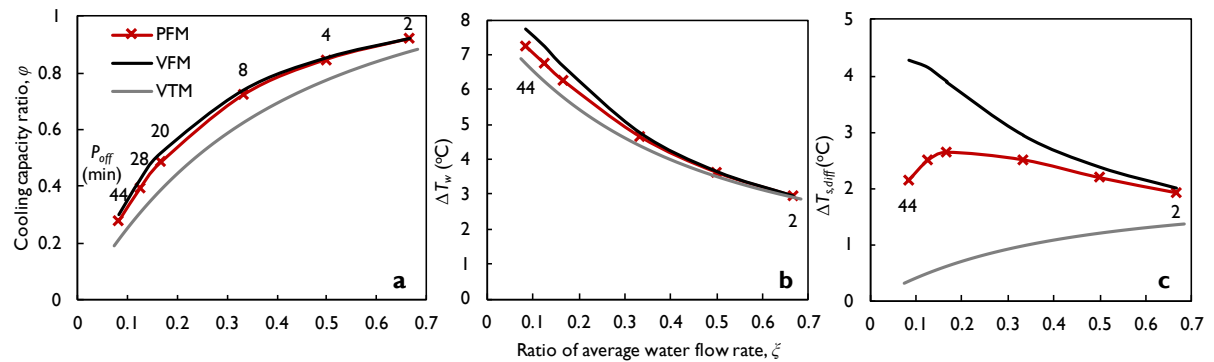


Fig. 7 Comparison of performance between different control methods: (a) Cooling capacity ratio; (b) supply and return water temperature difference; and (c) floor surface temperature non-uniformity (conditions for the PFM's off-time duration).

### 4.3 Sensitivity analysis on pulsed flow control

#### 4.3.1 Screening-based method

As the geometric and thermal properties of radiant slabs vary widely in engineering applications, we conducted a sensitivity analysis to identify the contribution of the individual design variables to the performance of the pulsed flow control method. We used the Morris method that is derived from one-factor-at-a-time screening-based methods, used to identify the subset of the main important input factors among a large number of input parameters by ranking input factors [38,39]. In the Morris method, only one parameter varies in every step and the final sensitivity measures are calculated by averaging at different points of the input space. Input factors are taken as a discrete number of values. Two sensitivity indexes can be obtained from it: (a) the average of the elementary effect ( $\mu$ ) estimates the main effect of the input factor on the output as a measure of importance for the input factor, (b) the standard deviation of the elementary effect ( $\sigma$ ) estimates the interaction with other factors, or the non-linear effects. We chose the Morris method for the sensitivity analysis because it is a general approach (model-independent), which achieves a good compromise between accuracy and efficiency [40]. Appendix A gives a detailed description of the Morris method.

In the sensitivity analysis, we defined the output as the capacity ratio with an identical ratio of the design water flow rate of 0.333. Where the reference case of CFM was designed with a supply and return water temperature of 16 °C and 18 °C, respectively and under an indoor operative temperature of 24 °C. We selected this as

the reference case as it is a realistic maximum capacity of the radiant slab in typical design practice. To study the effects of control and structural parameters, we selected two control parameters (design water flow rate and on-time duration) and eleven structural and thermal parameters of a radiant slab floor (pipe diameter, spacing and length, thickness, conductivity, specific heat and density of the surface and screed layer) in the sensitivity analysis. For each design parameter, we defined a uniform distribution from the minimum to the maximum value based on realistic extreme values (see Table 3). The number of elementary effects per design parameter ( $r$ ) is 10 in this paper. We fixed the pipe wall thickness at 2 mm in the sensitivity analysis. All of the combinations yield a reasonable pressure drop – the maximum pressure drop across the entire sensitivity analysis was 23 kPa.

Table 3 Range of design parameters for sensitivity analysis, ranked in order of decreasing sensitivity.

No.	Item	Unit	min	max
1	On-time duration	min	2	32
2	Pipe diameter	mm	15	25
3	Pipe spacing	mm	150	300
4	Surface layer conductivity	W/(m·K)	0.05	1.5
5	Design flow rate	m <sup>3</sup> /h	0.10	0.25
6	Screed layer thickness	mm	50	150
7	Screed layer conductivity	W/(m·K)	0.5	2
8	Surface layer thickness	mm	8	16
9	Pipe length	m	60	120
10	Screed layer specific heat	J/(kg·K)	500	1500
11	Screed layer density	kg/m <sup>3</sup>	1000	2500
12	Surface layer specific heat	J/(kg·K)	300	2500
13	Surface layer density	kg/m <sup>3</sup>	800	2000

Fig. 8 shows the results of the sensitivity analysis. The dashed wedge in Fig. 8 shows the following relation between the mean value and the standard deviation:

$$\sigma = \frac{\mu\sqrt{r}}{2} \quad (10)$$

If the point  $(\mu, \sigma)$  is inside the wedge, the design parameter has mainly a correlated or/and a non-linear impact on the ratio of cooling capacity. If the point for a design parameter is outside or far from the wedge, the impact can be considered as linear and a change in the design parameter would give a proportional change of the ratio of cooling capacity.

The three most important parameters have a mean elementary effect higher than 5.0 and are outside the wedge. Therefore, their effects on the cooling capacity ratio were nearly linear. It means the impact was almost the same across the whole parameter range. From the ranking of the mean values in the Morris method, we

conclude that the on-time duration ( $P_{on}$ ) has the highest mean value and therefore has a significant influence on the cooling capacity at the same average water flow rate. Among the eleven structure and thermal parameters, the water pipe diameter and spacing have a notable impact. Nevertheless, the structural and thermal property of the radiant slab floor, e.g., the thickness, conductivity, specific heat and density have little effect on the ratio of capacity of radiant slab floor. It is noteworthy that the design water flow rate of the PFMs did not much affect the ratio of capacity under the definition of such a reference case of the CFM with a supply and return water temperature difference of 2 °C. This may not be the case for systems designed with a lower flow rate and higher supply to return water temperature differential.

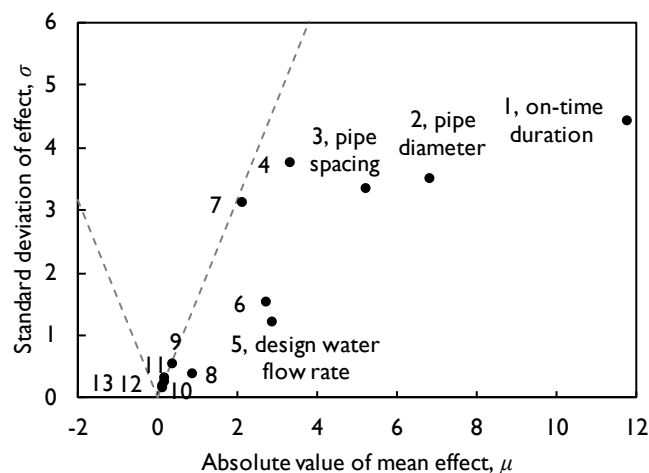


Fig. 8 Influence of design parameters on the cooling capacity ratio of radiant slab through Morris method.

#### 4.3.2 Evaluation of influencing factors on energy performance

The Morris method provides qualitative measures by ranking input factors, but it cannot quantify the effects of different factors on outputs. We further analyzed the effects of influencing factors on the ratio of cooling capacity under pulsed flow control. Focusing on the typical radiant slab described in Table 2, Fig. 9(a) shows the effect of the on-time duration on the ratio of capacity with a design water flow rate of 0.24 m<sup>3</sup>/h. With the same average water flow rate, the cooling capacity of the radiant slab floor increases with the decreasing on-time duration, and the upper bound is that of the VFM. Specifically, to achieve a cooling capacity ratio of 50%, the ratios of the required water flow rate for the intermittent control strategies with an on-time duration of 4 min, 10 min and 30 min were 17.7%, 20.5% and 24.3%, respectively. Meanwhile, the supply and return water temperature differences of the three conditions were 6.2 °C, 5.4 °C and 4.6 °C, respectively. Therefore, compared to previous intermittent control with an on-time duration of more than 30 min, the PFM with an on-time duration of 4 min requires 27% lower water flow rate and increases the supply and return water temperature difference by over 1.6 °C at 50% part load. In previous sensitivity analysis, experimental tests of a two-parameter switching control

---

were made by varying the switching interval from 10 to 60 min [20]. Results showed that better temperature regulation was achieved with short switching intervals under 40 min, according with the results of sensitivity analysis in this study.

In addition, Fig. 9(b) illustrates that the capacity ratio curves of PFMs with an on-time duration of 4 min and various design water flow rates are very similar to that of the VFM. The duration for the water to flush the pipe with a length of 120 m, and the design flow rate of 0.24 m<sup>3</sup>/h was 5 min. Therefore, the capacity of a radiant slab in PFM with an on-time duration less than or equal to the pipe flush time is approximately equal to that in VFM with the same average flow rate. Furthermore, the steady state heat transfer process of the VFM has analytical solutions reported by previous studies [35].

According to the results of sensitivity analysis, the water pipe diameter and spacing play an important role in the cooling capacity ratio of the PFM. In the following analysis, the PFMs were designed with an on-time duration of 4 min and the non-dimensional analysis was based on the reference case of the CFM with a supply and return water temperature difference of 2 °C. Fig. 9(c) shows the comparison of the capacity ratio between different pipe outer diameters for the radiant slab floor depicted in Table 2 except for a pipe wall thickness of 2 mm and a pipe spacing of 225 mm. With the same ratio of water flow rate, the cooling capacity ratio increased with increasing pipe diameter due to the increasing thermal mass of the water stored in the pipes. The deviation between the different pipe diameters increased with decreasing water flow rate. Fig. 9(d) shows the comparison of the cooling capacity ratio between different pipe spacing with a pipe inner and outer diameter of 16 and 20 mm, respectively. With the same flow rate ratio, the cooling capacity ratio increases with decreasing pipe spacing. Yet, the mean absolute deviation of the cooling capacity ratio between the pipe spacing of 150 and 300 mm was within 0.03. Therefore, the effects of other structure parameters and thermal properties of the radiant slab floor on the performance of the PFM were less than 0.03 and could be neglected.

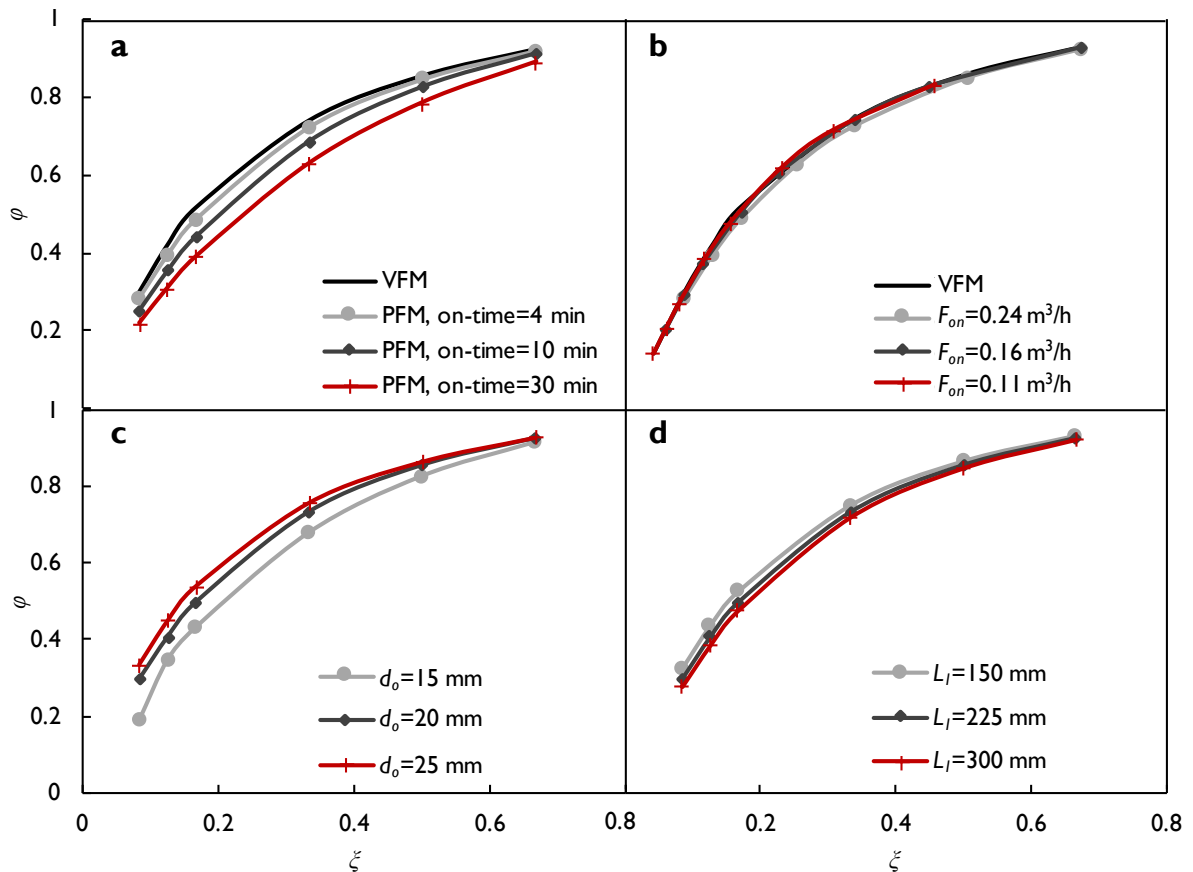


Fig. 9 Effects of influencing factors on the cooling capacity ratio in pulsed flow control methods: (a) On-time duration; (b) water flow rate in on-time duration; (c) water pipe diameter; and (d) pipe spacing.

## 5 Discussion

### 5.1 Practical application notes

First, it is worth noting that although the analysis above is for a cooling application, the pulsed flow control method applies equally well to both heating and cooling applications, and when the slab is in the floor and ceiling. The results of sensitivity analysis indicate that the capacity of the PFMs with an on-time duration less than the time taken to ‘flush’ the water in the pipe are almost identical to that of the VFM with the same average water flow rate whatever the structure and thermal property of the radiant slab are. Designing a system around this then requires knowledge of the ‘flush’ time for each radiant loop. In practice, it is better to simplify and choose the same on-time duration for all of the loops. Considering typical loop design characteristics ( e.g., a conventional pipe length of 120 m and a water velocity of 0.5 m/s), valve stroke times and valve on-off frequency, we suggest an on-time duration of 4 min. As shown in Fig. 9(a), the performances of the PFMs with an on-time duration less than 4 min are close. The advantages of using the PFM over the VFM are: a lower initial cost for the same size valve as a precision actuator is not

---

required; a more uniform surface temperature under part load conditions; and higher control precision at low part load conditions. In addition, the PFM brings forward higher request to the response time and durability of the two-position valve. The response time of the valve need to be short enough to keep the suggested on-time duration. The durability of the valve meets the requirements of the frequent valve on/off action.

It is worth considering the stability of the distribution system supplying water to the individual radiant zones in the building operating using PFM. Staggering the opening times of different radiant zones in the building would reduce pressure variation in the water circuit supplying those zones. For example, designers can easily achieve this behavior by fixing the available on/off ratios in equal increments of the on-time, and fixing the start of the control cycle differently by zone. For the 4 minute on-time recommended above, the PFM cycle would start in the first minute in zone 1, the second minute in zone 2, etc. and the possible on/off ratios are 4/0, 4/4, 4/8, 4/12, 4/16, etc.

### 5.2 Overall comparison of the three methods

According to the results above, we can provide an overall qualitative comparison of the three control methods: VFM, VTM and PFM. The simulation results indicate that the effect of the water flow rate is not great on the performance of the radiant slab in the VFM with a capacity ratio over 50%. It agrees with the results of previous sensitivity analysis on radiant slabs conducted by Jin et al[16]. As the modulating valve cannot regulate the water flow rate below 15% precisely, the VFM and VTM both have a low control precision at low part loads.

The PFM is able to control the capacity of radiant slabs with a high accuracy in a large range of part load from 10% to 90%. In addition, the required water flow rate and supply and return water temperature difference of the PFM is comparable to those of the VFM. Compared with the VFM, the PFM has a uniform surface temperature in part load. The energy efficiency of PFM is higher than that of the VTM, while the surface temperature non-uniformity of PFM is larger than that of the VTM.

From the point of view of the initial cost, the two-position valve and actuator used in the PFM are simpler and cheaper than the proportional valve and the precision actuator in the VFM, as well as the mixing valve and pump combination used in the VTM. In addition, the two-position valve is more robust and durable than the proportional valve, and the constant speed pumps coupled with radiant slabs in VTM increases the ongoing maintenance. Therefore, the PFM requires the lowest initial cost and maintenance among the three methods.

### 5.3 Limitations of this study

We analyzed the pulsed flow control method under periodic steady state conditions based on the assumption that the room thermal conditions are constant. In reality, these systems do not operate in periodic steady state, as the response time (at

---

63.2%) of the radiant slab is between 0.5 h and 6.0 h. Furthermore, many room conditions like building envelope, internal heat gains and solar radiation can affect the performance of the PFM. This study does not account for these factors. To do so requires a dynamic energy simulation program for the whole room that implements the full heat balance method (e.g., EnergyPlus), coupled with a detailed three-dimensional model of the radiant floor (such as we presented above). The value of the off-time should be determined online based on the feedback of the room operative temperature. Explicit algorithm of the PFM which consider the response time of the radiant slab due to its thermal mass and the load disturbance need to be proposed and evaluated in future work. Moreover, although we conducted an experiment for the purpose of initial model validation, a more comprehensive set of experiments could evaluate the performance of PFM at various part load rates, various on-time durations, and operating under dynamic conditions that accurately represent real building conditions. In addition, analysis in this study only focuses on the radiant slab with a single structural type.

## 6 Conclusions

Radiant slab systems are an energy efficient approach to provide high thermal comfort in buildings. In this paper, we propose a novel pulsed flow control method (PFM) for radiant slabs with a fixed (e.g. 4 minutes) on-time duration of the valve and variable off-time duration of the valve in one control cycle. We developed a 3D finite difference model of the radiant slab in order to capture the dynamic behavior of the PFM. We further conducted full-scale laboratory experiments using a radiant slab at FLEXLAB in Lawrence Berkeley National Laboratory, California, USA in order to evaluate the performance of the PFM and validate the 3D numerical model. We used this numerical model to simulate the capacity and temperature distribution within a radiant slab. We utilized a screening-based sensitivity analysis to identify the most important parameters in relation to energy performance in order to design and optimize the PFM. The main results of this study can be summarized as follows:

(1) The PFM is able to control the capacity of the radiant slab with a high accuracy over a large range of part loads from 10-90%, which avoids overcooling/overheating in part load. The PFM also achieves a high supply and return water temperature difference with a low average water flow rate. The PFM maintains an almost constant slab surface temperature under periodic steady state conditions due to the thermal inertia of the radiant slab.

(2) The results of the sensitivity analysis demonstrate that the most important factors on the PFM are the on-time duration, water pipe diameter and spacing. The geometrical and thermal parameters of radiant slabs have little effect on the non-dimensional capacity. The required water flow rate of the intermittent control increases with the on-time duration of the valve in the same capacity of the radiant slab. Compared to previous intermittent control strategies with an on-time duration of more than 30 min, the PFM requires 27% lower average flow rates while achieving the same 50% part load.

(3) Compared with the widely used variable temperature control method, the PFM requires 24% lower average water flow rate and attains higher supply to return water temperature differential under 50% load rate. The PFM allows the cooling/heating plant systems to operate more efficiently at warmer/cooler temperature. Compared with variable flow rate control method, the PFM achieves a similar capacity with the same average water flow rate, while it controls capacity more precisely and yields a more uniform surface temperature distribution in part load. Furthermore, the initial equipment cost required for the PFM is lower than for the VFM and the VTM.

## Appendix A. Description of the Morris Method

The radiant slab model can be represented by a function  $y(x)$  where  $y$  is the output variable of interest and  $x$  is a vector of real input variables with  $k$  coordinates. Input variables are transformed into reduced non-dimensional variables in the interval as  $x_i' = (x_i - x_{min}) / (x_{max} - x_{min})$ .  $x_{min}$  and  $x_{max}$  are the minimum and maximum of the input variable  $x_i$ , respectively. The domain of the vector  $x$  is then a hypercube  $H_k$  with unit length, a subset of  $R^k$ . For each reduced input variable, only discretized values are considered, using a  $p_i$  values regular grid:  $0, 1/(p_i-1), 2/(p_i-1), \dots, 1$ .

A simulation trajectory is defined as a sequence of  $(k+1)$  points in this hypercube, with each point differing from the preceding one by only one coordinate. Each input parameter only changes once in a trajectory with a pre-defined step  $\Delta_i$ . Morris suggested taking  $p$  even and  $\Delta_i = (p/2(p-1))$ .

The elementary effect  $EE$  for the  $i$ th input parameter in a point  $x$  is computed between the two points of the trajectory.

$$EE_i = \frac{y(x + e_i \Delta_i) - y(x)}{\Delta_i} \quad (A1)$$

$e_i$  is a vector of zeros but with its  $i$ th component equal to  $\pm 1$ . Each trajectory, with its  $(k+1)$  simulations, provides an estimate of the  $k$  elementary effects. The procedure is repeated  $r$  times creating a set of  $r \times (k+1)$  independent design parameters vectors. The model sensitivity to each design parameter is evaluated by the mean value ( $\mu$ ) and the standard deviation ( $\sigma$ ) of the elementary effects:

$$\mu_i = \frac{1}{r} \sum_{t=1}^r EE_{it} \quad (A2)$$

$$\sigma_i = \sqrt{\frac{1}{(r-1)} \sum_{t=1}^r (EE_{it} - \mu_i)^2} \quad (A3)$$

The result of the sensitivity analysis is a list of important design parameters and a ranking of the design parameters by the strength of their impact on the output,  $\mu$ .

---

## Acknowledgments

This research described in this paper was supported by the National Natural Science Foundation of China (No.51638010, No.51521005), the China Scholarship Council (No. 201606210234) and the California Energy Commission (CEC) Electric Program Investment Charge (EPIC) (EPN-14-009) “Optimizing Radiant Systems for Energy Efficiency and Comfort”, and the Center for the Built Environment, University of California, Berkeley.

## References

- [1] K.-N. Rhee, K.W. Kim, A 50 year review of basic and applied research in radiant heating and cooling systems for the built environment, *Build. Environ.* 91 (2015) 166–190. doi:10.1016/j.buildenv.2015.03.040.
- [2] R. Hu, J.L. Niu, Operation dynamics of building with radiant cooling system based on Beijing weather, *Energy Build.* 151 (2017) 344–357. doi:10.1016/j.enbuild.2017.06.068.
- [3] R. Hu, J.L. Niu, A review of the application of radiant cooling & heating systems in Mainland China, *Energy Build.* 52 (2012) 11–19. doi:10.1016/j.enbuild.2012.05.030.
- [4] P. Ma, L.-S. Wang, N. Guo, Modeling of hydronic radiant cooling of a thermally homeostatic building using a parametric cooling tower, *Appl. Energy.* 127 (2014) 172–181. doi:10.1016/j.apenergy.2014.04.031.
- [5] J.I. Villarino, A. Villarino, F.Á. Fernández, Experimental and modelling analysis of an office building HVAC system based in a ground-coupled heat pump and radiant floor, *Appl. Energy.* 190 (2017) 1020–1028. doi:10.1016/j.apenergy.2016.12.152.
- [6] H.E. Feustel, C. Stetiu, Hydronic radiant cooling — preliminary assessment, *Energy Build.* 22 (1995) 193–205. doi:10.1016/0378-7788(95)00922-K.
- [7] G.P. Henze, C. Felsmann, D.E. Kalz, S. Herkel, Primary energy and comfort performance of ventilation assisted thermo-active building systems in continental climates, *Energy Build.* 40 (2008) 99–111. doi:10.1016/j.enbuild.2007.01.014.
- [8] Z. Tian, J.A. Love, Energy performance optimization of radiant slab cooling using building simulation and field measurements, *Energy Build.* 41 (2009) 320–330. doi:10.1016/j.enbuild.2008.10.002.
- [9] B.A. Thornton, W. Wang, M.D. Lane, R. Michael I., B. Liu, Technical Support Document: 50% Energy Savings Design Technology Packages for Medium Office Buildings., Pacific Northwest National Laboratory, Richland, WA, USA, 2009.
- [10] E.M. Saber, K.W. Tham, H. Leibundgut, A review of high temperature cooling systems in tropical buildings, *Build. Environ.* 96 (2016) 237–249. doi:10.1016/j.buildenv.2015.11.029.

- 
- [11] J.-M. Seo, D. Song, K.H. Lee, Possibility of coupling outdoor air cooling and radiant floor cooling under hot and humid climate conditions, *Energy Build.* 81 (2014) 219–226. doi:10.1016/j.enbuild.2014.06.023.
- [12] Z. Tian, J.A. Love, A field study of occupant thermal comfort and thermal environments with radiant slab cooling, *Build. Environ.* 43 (2008) 1658–1670. doi:10.1016/j.buildenv.2007.10.012.
- [13] J. Le Dréau, P. Heiselberg, Sensitivity analysis of the thermal performance of radiant and convective terminals for cooling buildings, *Energy Build.* 82 (2014) 482–491. doi:10.1016/j.enbuild.2014.07.002.
- [14] Tsinghua University Building Energy Research Center, 2008 Annual Report on China Building Energy Efficiency, China Architecture & Building Press, Beijing, 2008.
- [15] M. Zaheer-uddin, Z.L. Zhang, S.H. Cho, Augmented control strategies for radiant floor heating systems, *Int. J. Energy Res.* 26 (2002) 79–92. doi:10.1002/er.767.
- [16] X. Jin, X. Zhang, Y. Luo, R. Cao, Numerical simulation of radiant floor cooling system: The effects of thermal resistance of pipe and water velocity on the performance, *Build. Environ.* 45 (2010) 2545–2552. doi:10.1016/j.buildenv.2010.05.016.
- [17] J.-H. Lim, J.-H. Jo, Y.-Y. Kim, M.-S. Yeo, K.-W. Kim, Application of the control methods for radiant floor cooling system in residential buildings, *Build. Environ.* 41 (2006) 60–73. doi:10.1016/j.buildenv.2005.01.019.
- [18] L. Liu, L. Fu, Y. Jiang, A new “wireless on-off control” technique for adjusting and metering household heat in district heating system, *Appl. Therm. Eng.* 36 (2012) 202–209. doi:10.1016/j.applthermaleng.2011.11.040.
- [19] C.-S. Kang, C.-H. Hyun, M. Park, Fuzzy logic-based advanced on-off control for thermal comfort in residential buildings, *Appl. Energy.* 155 (2015) 270–283. doi:10.1016/j.apenergy.2015.05.119.
- [20] S.-H. Cho, M. Zaheer-uddin, An experimental study of multiple parameter switching control for radiant floor heating systems, *Energy.* 24 (1999) 433–444. doi:10.1016/S0360-5442(98)00101-7.
- [21] M. Gwerder, J. Tödtli, B. Lehmann, V. Dorer, W. Güntensperger, F. Renggli, Control of thermally activated building systems (TABS) in intermittent operation with pulse width modulation, *Appl. Energy.* 86 (2009) 1606–1616. doi:10.1016/j.apenergy.2009.01.008.
- [22] M. Gwerder, B. Lehmann, J. Tödtli, V. Dorer, F. Renggli, Control of thermally-activated building systems (TABS), *Appl. Energy.* 85 (2008) 565–581. doi:10.1016/j.apenergy.2007.08.001.
- [23] S.H. Cho, M. Zaheer-uddin, Predictive control of intermittently operated radiant floor heating systems, *Energy Convers. Manag.* 44 (2003) 1333–1342. doi:10.1016/S0196-8904(02)00116-4.
- [24] J. (Dove) Feng, F. Chuang, F. Borrelli, F. Bauman, Model predictive control of radiant slab systems with evaporative cooling sources, *Energy Build.* 87 (2015) 199–210. doi:10.1016/j.enbuild.2014.11.037.

- 
- [25] B.-C. Ahn, J.-Y. Song, Control characteristics and heating performance analysis of automatic thermostatic valves for radiant slab heating system in residential apartments, *Energy*. 35 (2010) 1615–1624. doi:10.1016/j.energy.2009.11.007.
- [26] R. Holopainen, P. Tuomaala, J. Piippo, Uneven gridding of thermal nodal networks in floor heating simulations, *Energy Build.* 39 (2007) 1107–1114. doi:10.1016/j.enbuild.2006.12.006.
- [27] D. Wang, Y. Liu, Y. Wang, J. Liu, Numerical and experimental analysis of floor heat storage and release during an intermittent in-slab floor heating process, *Appl. Therm. Eng.* 62 (2014) 398–406. doi:10.1016/j.applthermaleng.2013.09.028.
- [28] T. Weber, G. Jóhannesson, M. Koschenz, B. Lehmann, T. Baumgartner, Validation of a FEM-program (frequency-domain) and a simplified RC-model (time-domain) for thermally activated building component systems (TABS) using measurement data, *Energy Build.* 37 (2005) 707–724. doi:10.1016/j.enbuild.2004.10.005.
- [29] P. Ma, L.-S. Wang, N. Guo, Modeling of TABS-based thermally manageable buildings in Simulink, *Appl. Energy*. 104 (2013) 791–800. doi:10.1016/j.apenergy.2012.12.006.
- [30] Z. Tian, B. Duan, X. Niu, Q. Hu, J. Niu, Establishment and experimental validation of a dynamic heat transfer model for concrete radiant cooling slab based on reaction coefficient method, *Energy Build.* 82 (2014) 330–340. doi:10.1016/j.enbuild.2014.07.031.
- [31] R.K. Strand, Heat source transfer functions and their application to low temperature radiant heating systems, Ph.D. Thesis, University of Illinois at Urbana-Champaign, USA, 1995.
- [32] H. Tang, X.-H. Liu, Y. Jiang, Theoretical and experimental study of condensation rates on radiant cooling surfaces in humid air, *Build. Environ.* 97 (2016) 1–10. doi:10.1016/j.buildenv.2015.12.003.
- [33] Department of Energy's FLEXLAB at Lawrence Berkeley National Laboratory, (n.d.). <https://flexlab.lbl.gov/>.
- [34] M.S. Shin, K.N. Rhee, S.R. Ryu, M.S. Yeo, K.W. Kim, Design of radiant floor heating panel in view of floor surface temperatures, *Build. Environ.* 92 (2015) 559–577. doi:10.1016/j.buildenv.2015.05.006.
- [35] J.P. Holman, S. Bhattacharyya, *Heat Transfer (In SI Units)*, (Tenth Edition), Tata McGraw-Hill Education Pvt. Ltd, 2011.
- [36] B. Ning, S. Schiavon, F.S. Bauman, A novel classification scheme for design and control of radiant system based on thermal response time, *Energy Build.* 137 (2017) 38–45. doi:10.1016/j.enbuild.2016.12.013.
- [37] ASHRAE handbook: fundamentals, in *Heat, Air, and Moisture Control in Buildings Assemblies- Material Properties*, in: American Society of Heating, Air-Conditioning and Refrigeration Engineers, Atlanta, GA, 2009.
- [38] P. Heiselberg, H. Brohus, A. Hesselholt, H. Rasmussen, E. Seinre, S. Thomas, Application of sensitivity analysis in design of sustainable buildings,

---

Renew. Energy. 34 (2009) 2030–2036. doi:10.1016/j.renene.2009.02.016.

[39] D. Garcia Sanchez, B. Lacarrière, M. Musy, B. Bourges, Application of sensitivity analysis in building energy simulations: Combining first- and second-order elementary effects methods, *Energy Build.* 68, Part C (2014) 741–750. doi:10.1016/j.enbuild.2012.08.048.

[40] W. Tian, A review of sensitivity analysis methods in building energy analysis, *Renew. Sustain. Energy Rev.* 20 (2013) 411–419. doi:10.1016/j.rser.2012.12.014.